Semiclassical trajectory perspective of glory rescattering in strong-field photoelectron holography

L. G. Liao [1,2] Q. Z. Xia,[3,*] J. Cai [4] and J. Liu [2,5,†]

[1]*School of Physics, Peking University, Beijing 100871, China*

[2]*CAPT, HEDPS, and IFSA Collaborative Innovation Center of MoE, Peking University, Beijing 100871, China*

[3]*National Laboratory of Science and Technology on Computational Physics, Institute of Applied Physics and Computational Mathematics, Beijing 100088, China*

[4]*School of Physics and Electronic Engineering, Jiangsu Normal University, Xuzhou 221116, China*

[5]*Graduate School of China Academy of Engineering Physics, Beijing 100193, China*

(Received 18 December 2021; revised 18 February 2022; accepted 4 May 2022; published 17 May 2022)

We investigate theoretically the photoelectron momentum distribution (PMD) of ionized atoms irradiated by a linearly polarized intense laser, focusing on the holography interference patterns in PMD that carry important information of the initial wavefunction of a tunneled electron and its experienced atomic potential in rescattering. With the help of Dyson series and a semiclassical propagator, we calculate the scattering amplitudes in the cylindrical coordinate representation. In contrast to conventional recognitions that photoelectron holography is the interference of two branches of electron trajectories, however, we find strikingly that infinitely many semiclassical trajectories can be deflected by the combined Coulomb potential and laser field into the same final momentum. The initial momenta are found to be distributed on a ring-shaped curve in the transverse momentum plane and the initial positions of these trajectories are perpendicular to their initial momentum vectors. For the zero final transverse momentum, the above ring-source trajectories degenerate into the point-source axial caustic trajectories (or glory trajectories) and the quantum interference of these trajectories will dramatically alter the scattering amplitudes, which is termed the glory rescattering effect. By following Berry's spirit of uniform approximation for glory scattering in optics, we can finally derive a uniform formulation of the rescattering amplitude in the Bessel functions for the strong-field photoelectron holography patterns. Our results are in good agreement with solutions of the time-dependent Schrödinger equation and can account for recent photoelectron holography experiments. Important applications of our theory are also discussed.

DOI: 10.1103/PhysRevA.105.053115

I. INTRODUCTION

Strong-field photoelectron holography (SFPH) provides a powerful tool for investigating the structure and dynamics of atoms and molecules [1–14]. The physics behind SFPH is that in analogy to conventional optical holography, the modulation patterns in photoelectron momentum distribution (PMD) are the phase interference of diverse electron trajectories and therefore carry important information about the initial states of tunneled electrons and their experienced rescattering potentials [15–17]. Nevertheless, to correctly extract the information contained in the holographic patterns of PMDs, sophisticated nonperturbative theories for the photoionization and rescattering in combined Coulombic and intense laser fields are required.

Semiclassical dynamics can provide intuitive pictures for the strong-field ionization and has successfully explained the physical mechanisms behind many striking structures in PMD spectroscopy [18–22]. In the semiclassical description, the photoelectron experiences tunneling through the electromagnetic field suppressed Coulomb barrier and is then accelerated in the combined laser field and the Coulomb potential of its parent ion. The latter process is known as rescattering or recollision. SFPH is tightly related to the quantum interference in the rescattering process [23–27]. Numerically, PMDs can be obtained by directly integrating the time-dependent Schrödinger equation (TDSE) [3,8,28,29] in full dimensionality (three dimensions). Theoretically, quantum scattering theory based on strong-field approximation (SFA) [30–32] as well as the Coulomb corrected strong field approximation (CCSFA) [33–36] has been successfully exploited to understand many interesting structures of PMDs. More recently, Gouy's phase anomaly [37] and Maslov's phase [38] in strong-field rescattering trajectories are addressed [39]. In the above discussions, two branches of trajectories, the directly ionized trajectory and the the rescattering trajectory, are considered. However, due to the existence of caustic singularity [40,41], the scattering theories that coherently sum over two trajectories for each asymptotic momentum fail to analyze the glory effect, in which the contribution of infinitely many trajectories can dramatically modulate the scattering amplitude. In order to resolve this caustic singularity, glory rescattering theory (GRT) has been developed [42]. According to the GRT, infinitely many semiclassical trajectories are integrated to give rise to a pattern of Bessel function distribution. The results of the GRT are also certificated by recent two-step

*xia_qinzhi@iapcm.ac.cn

†jliu@gscaep.ac.cn

model calculations [27]. Nevertheless, the GRT focuses on caustic singularity, i.e., the near-zero final transverse momentum region in PMDs. To extend the GRT to the nonzero final transverse momentum region and give a uniform description of PMDs from the semiclassical trajectory perspective is urgently needed for practical SFPH applications.

On the other hand, Berry in the 1960s applied a uniform approximation theory to solve the glory scattering problems in optics and developed a scattering amplitude formula that can be continually applied from small-angle scattering to large-angle scattering or even backscattering [43,44]. Following the concept of the uniform approximation, in the present work we extend the GRT by exploiting a semiclassical path integral to deduce a uniform formulation for all angles of forward and backward rescattering in PMDs. Our results are compared with TDSE calculations, the existing theories as well as the holography experiments.

The paper is organized as follows. In Sec. II, we present our theoretical formulation. Section III contains our results and discussions. Atomic units are used unless otherwise specified.

II. THEORETICAL FORMULISM

A. Scattering amplitude from the semiclassical trajectory perspective

We start with the Hamiltonian for the atom-field interaction problem in the length gauge, which takes the following form of $H[\vec{r}(t),\vec{p}(t)]=\frac{p^2(t)}{2}+\vec{F}(t)\cdot\vec{r}(t)-\frac{1}{r(t)}$. By exploiting the Dyson series [45], we have $U(t,0)=U_0(t,0)-i\int_0^t dt_0U(t,t_0)V_L(t_0)U_0(t_0,0)$, where U denotes the complete evolution operator in the combined Coulomb potential and laser field; U_0 represents the evolution operators under pure Coulomb potential, and has the property of $U_0(t_0,0)|\psi(0)\rangle=|\psi(0)\rangle e^{iI_pt_0}$. Here I_p is the ionization potential and $|\psi(0)\rangle$ denotes the initial wavefunction; $V_L=\vec{F}(t)\cdot\vec{r}$ and $\vec{F}(t)$ is the electric field.

With the help of Dyson's series, we thus have the time-dependent wavefunction $|\psi(t)\rangle=U_0(t,0)|\psi(0)\rangle-i\int_0^t dt_0U(t,t_0)V_L(t_0)U_0(t_0,0)|\psi(0)\rangle$. The scattering amplitude of a continuum state with asymptotic momentum $\vec{p}_f$ can be written as $M_{\vec{p}_f}=\langle\vec{p}_f|\psi(t_f)\rangle=-i\int dt_0\langle\vec{p}_f|U(t_f,t_0)V_L(t_0)U_0(t_0,0)|\psi(0)\rangle$ with $t_f\to\infty$. With inserting an identity $\int d\vec{p}_0|\vec{p}_0\rangle\langle\vec{p}_0|\equiv 1$, we have

$$M_{\vec{p}_f}=-i\iint dt_0d\vec{p}_0G(\vec{p}_f,t_f;\vec{p}_0,t_0)\mathcal{D}(\vec{p}_0,t_0)e^{iI_pt_0}. \quad (1)$$

Here $\mathcal{D}(\vec{p}_0,t_0)=\langle\vec{p}_0|V_L(t_0)|\psi(0)\rangle$ represents the dipole matrix element and the momentum-to-momentum propagator $G(\vec{p}_f,t_f;\vec{p}_0,t_0)=\langle\vec{p}_f|U(t_f,t_0)|\vec{p}_0\rangle$.

In semiclassical approximation [38,46,47], the propagator $G(\vec{p}_f,t_f;\vec{p}_0,t_0)=\mathcal{F}(\vec{p}_f,t_f;\vec{p}_0,t_0)e^{i\mathcal{S}(\vec{p}_f,t_f;\vec{p}_0,t_0)}$, where the semiclassical phase $\mathcal{S}(\vec{p}_f,t_f;\vec{p}_0,t_0)=\int_{t_0}^{t_f}dt(-\vec{r}(t)\cdot\dot{\vec{p}}(t)-H[\vec{r}(t),\vec{p}(t)])$. We neglect the Maslov phase in holography patterns, and the reason is discussed in Sec. II C. The prefactor $\mathcal{F}=[\frac{1}{(2\pi i)^3}\det(\frac{\partial^2\mathcal{S}}{\partial p_0\partial p_f})]^{\frac{1}{2}}$.

The semiclassical operator only contains the leading term in an $\hbar^n$ expansion. The semiclassical approximation is expected to be valid when the scale of the particle wavepacket is much smaller than the typical spatial scale or for the motion with continuous energy spectrums. This is the case for the electron rescattering processes including the hard rescattering. However, it is difficult to precisely elucidate the validity range of the semiclassical propagator in strong-field physics. Some detailed discussions on the topic can be found in Refs. [47,56].

Considering the case of a linearized laser field that is polarized along the z axis, the problem intrinsically has rotational symmetry about the axial coordinate. We therefore introduce the cylindrical coordinates instead of Cartesian coordinates. Thus, Eq. (1) can be rewritten as

$$M_{\vec{p}_f}=\iiiint dt_0dp_{z0}dp_{\rho0}d\phi p_{\rho0}\mathcal{F}\cdot\mathcal{D}\cdot e^{i\mathcal{A}(\vec{p}_f,t_f;\vec{p}_0,t_0)}. \quad (2)$$

Here, $\mathcal{A}=\mathcal{S}+I_pt_0$. Because $\mathcal{F}$ and $\mathcal{D}$ are slowly varying functions, we treat Eq. (2) with the steepest descent method for the time integration as well as the momentum integrations. The saddle-point condition for the time variable gives

$$\left.\frac{\partial\mathcal{A}}{\partial t_0}\right|_{t_s}=0. \quad (3)$$

By applying the steepest-descent method to treat the integration on p_{z0} and $p_{\rho0}$, we obtain the coordinates of the saddle points satisfying

$$z(t_s)=0,\quad \vec{p}_s\cdot\vec{p}_{\rho s}=0. \quad (4)$$

In the above deductions, we use the relation $\frac{\partial\mathcal{A}}{\partial p_\rho}=x\cos\phi+y\sin\phi=\vec{\rho}\cdot\vec{p}_\rho/|p_\rho|$. In contrast to the conventional steepest-descent method implemented in the Cartesian coordinates, in which the saddle-point conditions give that the positions of the saddle points are located at the origin, in our cylindrical coordinate representation, the saddle points might even not be on the symmetric z axis. The second formula in Eq. (4) gives a constraint on the initial coordinates and momenta.

Then the scattering amplitude here becomes

$$M_{\vec{p}_f}\approx\int d\phi p_{\rho_s}\left(\frac{(2\pi i)^3}{\det\left(\frac{\partial^2\mathcal{A}}{\partial(t_0,p_{z0},p_{\rho0})}\big|_s\right)}\right)^{\frac{1}{2}}\mathcal{F}_s\mathcal{D}_se^{i\mathcal{A}_s}, \quad (5)$$

where $\mathcal{A}_s$, $\mathcal{F}_s$, and $\mathcal{D}_s$ represent the values at the saddle point $(\vec{p}_s,t_s)$.

In the above integration, the phase $\mathcal{A}_s$ is the implicit function of the azimuthal angle ϕ. To treat this scattering amplitude integration, we closely follow Berry's spirit of uniform approximation [43,44] with renormalizing the angular variable. Let us introduce a new angular variable φ, which satisfies $\phi=0\leftrightarrow\varphi=0$, $\phi=\pi\leftrightarrow\varphi=\pi$, and $\mathcal{A}_s(\phi)=\bar{\mathcal{A}}_s(\varphi)\equiv\mathcal{A}_0+\mathcal{A}_1\cos(\varphi)$, where $\mathcal{A}_0=(\mathcal{A}_s(\phi=0)+\mathcal{A}_s(\phi=\pi))/2$ corresponds to the sum of the phases of the $\phi=0$ and $\phi=\pi$ semiclassical photoelectron trajectories, and $\mathcal{A}_1=(\mathcal{A}_s(\phi=0)-\mathcal{A}_s(\phi=\pi))/2$ corresponds to the phase difference between the $\phi=0$ and $\phi=\pi$ trajectories.

With the variable transformation, the scattering amplitude of Eq. (5) turns out to be (see Appendix A for details)

$$M_{\vec{p}_f}\approx\int_0^{2\pi}d\varphi C(\varphi)e^{i(\mathcal{A}_0+\mathcal{A}_1\cos\varphi)}. \quad (6)$$

The prefactor $C(\varphi)$ takes the form

$$C(\varphi) \propto \frac{\mathcal{D}_s}{\sqrt{\frac{d^2\mathcal{A}_s}{dt_s^2}}}(\mathcal{A}_1\cos\varphi)^{\frac{1}{2}}\frac{p_{\rho s}}{p_{\rho f}}\det\left(\frac{\partial(p_{zs},p_{\rho s})}{\partial(p_{zf},p_{\rho f})}\right). \quad (7)$$

We can approximate the above function in the following form: $C(\varphi)\approx\frac{1}{2}(C(0)+C(\pi))+\frac{1}{2}(C(0)-C(\pi))\cos\varphi$. Finally, the scattering amplitude integration can be evaluated by the Bessel functions in the following explicit forms, which is termed the uniform glory rescattering theory (UGRT):

$$\begin{aligned} M_{\vec{p}_f} &\approx \frac{1}{2}\int_0^{2\pi} d\varphi[(C(0)+C(\pi))+(C(0) \\ &\quad -C(\pi))\cos\varphi]e^{i\mathcal{A}_1\cos\varphi} \\ &= \frac{1}{2}(C(0)+C(\pi))J_0(\mathcal{A}_1)-\frac{1}{2}i(C(0)-C(\pi))J_1(\mathcal{A}_1). \end{aligned} \quad (8)$$

Let us now analyze the physics behind the above deductions. From the expression of Eq. (5), we see that for a given final photoelectron momentum, in contrast to conventional recognition of the two-trajectory interference, we find that infinitely many semiclassical trajectories can be deflected by the combined Coulomb potential and laser field into the same final momentum. This phenomenon was mentioned very recently only for the case of zero final transverse momentum [42], where the infinitely many trajectories of tunneling electrons at moment $\mathrm{Re}(t_s)$ on the z axis with equal transverse momentum are rescattered to the final states with zero transverse momentum, leading to so-called caustic singularity [48]. A similar phenomenon is termed the glory scattering, first discussed in optics and then extended to particle scattering by Wheeler [41,49,50]. The quantum interference of the infinitely many glory trajectories will manipulate the scattering amplitude, showing a bright fringe around the zero angle in SFPH. This picture is apparent and can be readily imagined by considering the cylindrical symmetry of the geometric configuration of the problem.

Our above deductions explicitly indicate that the infinite-trajectory interference can emerge also for nonzero final transverse momenta. According to Eq. (4) and from our detailed calculations of these semiclassical trajectories (see Figs. 1 and 2 in the following section), we find that the initial positions of these trajectories are no longer on the symmetric z axis and are found to be distributed on a ring-shaped curve in the transverse coordinate plane. The initial transverse momenta are perpendicular to the initial position vectors according to the constraint of Eq. (4).

Moreover, the expression of Eq. (8) shows that the scattering amplitude can be expressed in the sum of zero-order and first-order Bessel functions in uniform approximation. The variable $\mathcal{A}_1$ in the Bessel functions represents the phase difference of two distinct semiclassical trajectories corresponding to $\phi=0$ and $\phi=\pi$, respectively. When the final transverse momentum tends to zero, $C(0)$ equals $C(\pi)$, and Eq. (8) will reduce to the formulation of GRT in Ref. [42]. In GRT, $M_{\vec{p}}$ can be written in the form $|M_{\vec{p}}|^2\sim\varpi\, p_{\perp g}b_g J_0^2(p_{\perp}b_g)$ in which $p_{\perp g}$ is the initial transverse momentum of the glory trajectory at the tunneling exit, b_g is the emergent impact parameter of the glory trajectory, and ϖ is the weight of the glory trajectory.

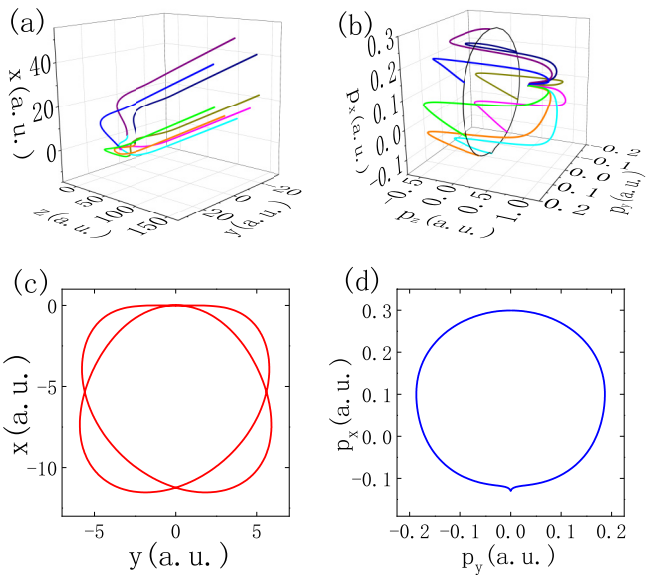

FIG. 1. Photoelectron semiclassical trajectories in (a) coordinate space and (b) momentum space for the final state of $p_{zf}=0.66$ a.u., $p_{xf}=0.12$ a.u., $p_{yf}=0$. (c) The initial positions on the projected x-y plane and (d) the initial transverse momenta on the projected p_x-p_y plane. The laser parameters are $\lambda=1200$ nm and $I=8.7\times10^{13}$ W/cm^2.

In this situation, we note that the phase difference of $\mathcal{A}_1$ in Eq. (8) approximately equals $p_{\perp}b_g$; here $p_{\perp}$ is the final transverse momentum.

Note that various alternative semianalytical methods have been used in strong-field ionization, such as the improved SFA (ISFA), various versions of the CCSFA, and the analytical R matrix (ARM) [13]. In the semiclassical framework, we exploit the semiclassical evolution operator G in Eq. (1) which includes all the interactions that photoelectrons undergo in the ionization and rescattering processes, while in ISFA, Dyson's series is iterated by using an approximate evolution operator that usually only contains the laser field. In particular, we find that infinitely many semiclassical paths can approach the same final momentum, and the quantum interference of these trajectories will dominate the holographic fringe structure. In contrast to CCSFA, our theory properly takes into account the contributions of these infinitely many paths by using uniform approximation. Our semiclassical approach differs from the ARM method [51,52] that splits the space into an inner and outer region and only in the outer region the concept of quantum trajectories is employed.

B. Calculations of semiclassical trajectories and associated phase accumulations

States at some typical times that an electron experiences in its ionization process are listed in Table I, in which $\mathrm{Re}(t_s)$ is the real part of saddle-point time t_s. The condition of the saddle point according to Eq. (3) is obtained by solving the saddle-point equation within the strong-field approximation (see, e.g., Refs. [53,54]) $\frac{1}{2}(\tilde{p}_{\rho s}^2+[\tilde{p}_{zs}+A(t_s)]^2)+I_p=0$, where $\tilde{p}$ is the canonical momentum. The corresponding

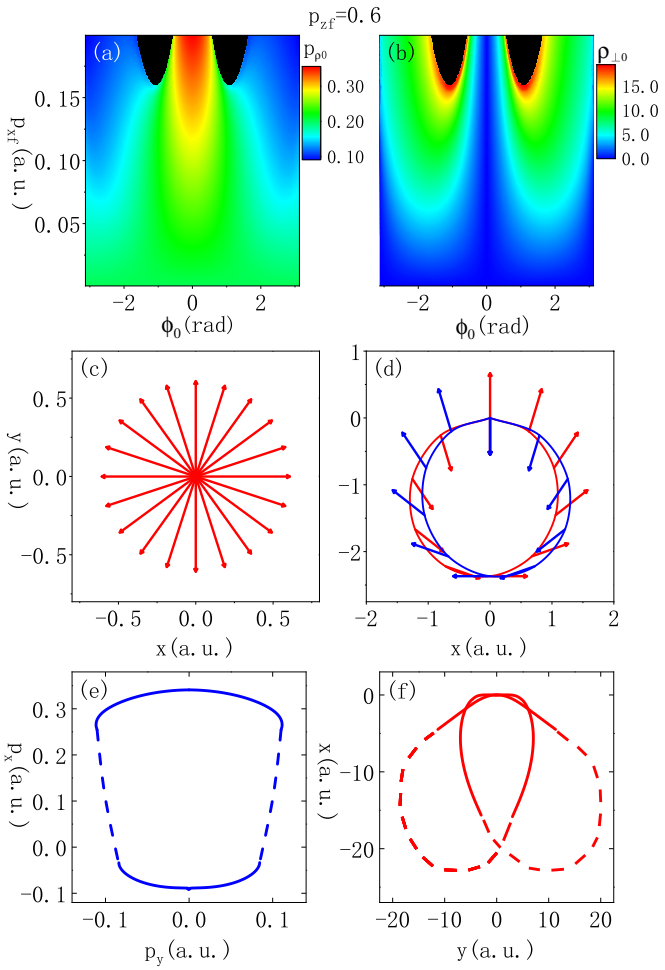

FIG. 2. For $p_{zf} = 0.6$ a.u., $p_{yf} = 0$, and p_{xf} varied from 0 to 0.2 a.u., we present (a) the calculated initial transverse momentum of $p_{\rho 0}$ depending on azimuthal angle of ϕ_0, and (b) the initial displacement of ρ_0 to the z axis depending on azimuthal angle of ϕ_0. (c) For $p_{xf} = 0$ corresponding to the glory caustic singularity, the initial positions are exactly at the origin of the projected x-y plane; the initial transverse momenta are schematically shown by arrows. (d) The same as (c) but $p_{xf} = 0.03$ a.u. (e) The initial transverse momenta of photoelectron trajectories when $p_{xf} = 0.2$ a.u., and (f) the corresponding initial positions on the projected x-y plane. The black areas in (a) and (b) represent the classical trajectory forbidden regions. The dashed lines in (e) and (f) are the analytical extensions of the solutions to the forbidden regions. The laser parameters are $\lambda = 1200$ nm and $I = 8.7 \times 10^{13}$ W/cm^2.

kinetic momenta at the saddle point are then given by $p_{zs} = \tilde{p}_{zs} + A(t_s)$ and $p_{\rho s} = \tilde{p}_{\rho s}$.

Under the constraint of the saddle-point condition of Eq. (4), for a given final momentum, we can use shooting method [55] to obtain the initial conditions of semiclassical trajectories by solving the following Newton equations of motion numerically using the Runge-Kutta-Fehlberg method: $\dot{\vec{p}} = -\vec{F}(t) - \vec{\nabla} V(\vec{r}(t))$, where $V(\vec{r}(t))$ is the atomic potential. The asymptotic condition is that $t \to \infty$, $\vec{p} \to \vec{p}_f$. In semiclassical treatment, the phase of each trajectory is divided into two parts: An ionization process phase and an acceleration process phase. The phase

TABLE I. States of an electron in ionization process.

Time	State description	Position and/or momentum
t_s	Saddle point	$z_s = 0, \vec{p}_s \cdot \vec{p}_{\rho s} = 0, \vec{p}_{zs}, \vec{p}_{\rho s}$
$\mathrm{Re}(t_s)$	Tunneling exit	$\vec{r}_0 = \mathrm{Re}\int_{t_s}^{\mathrm{Re}(t_s)} (\tilde{\vec{p}} + A(t))dt, \vec{p}_s$
$t_f = \infty$	Final state	$\vec{p}_f, \dot{\vec{p}} = -\vec{F}(t) - \vec{\nabla} V(r(\vec{t}))$

accumulated during the ionization process is given by $\mathcal{A}(t_s \to \mathrm{Re}(t_s)) = -\frac{1}{2}\int_{t_s}^{\mathrm{Re}(t_s)} (\tilde{p}_{\rho s}^2 + [\tilde{p}_{zs} + A(t)]^2)\, dt$. The phase accumulated during the acceleration process can be expressed as $\mathcal{A}(t_f; \mathrm{Re}(t_s)) = -\int_{\mathrm{Re}(t_s)}^{t_f} dt\{\dot{\vec{p}}(t) \cdot \vec{r}(t) + H[\vec{r}(t), \vec{p}(t)]\}$ [56].

With these semiclassical trajectories and corresponding phases, we can reconstruct the photoelectron momentum spectrum according to Eq. (8).

C. Some remarks

In conventional treatments, one directly treats the integral of Eq. (1) with the steepest-descent method for all momentum variables in Cartesian coordinates; the initial positions of a tunneled electron will locate on the z axis. Then, within half a laser cycle there are usually two trajectories (one is the directly ionized trajectory, the other is the rescattering trajectory) that can reach the same final momentum. The two-trajectory interference is used to explain the SFPH where the modulation fringe can be expressed in the cosine function of the phase difference between the two trajectories. Recently, the Gouy phase [37] was introduced to the two-trajectory strong-field interference picture in a three-dimensional (3D) model to compensate for the divergence of the preexponential factors of the semiclassical propagator at focal points [39]. As a result, the phase difference in the cosine function will be modified by a $\nu\pi/2$ phase, where ν is the Maslov index [57–60]. In fact, due to the cylindrical symmetry of the problem, infinitely many ring-source trajectories can converge to the same final momentum state. The quantum interference of the ring-source trajectories will give rise to the pattern in PMDs of Bessel functions instead of cosine functions. Within the framework of UGRT, the Maslov phases of different trajectories vanish. This is because in the representation of cylindrical coordinates, due to the cylindrical symmetry, the system is essentially reduced to a two-dimensional (2D) problem under the uniform approximation, in which the preexponential factors of the semiclassical propagator keep finite along the rescattering trajectories (i.e., no focal points) according to our detailed calculations.

III. APPLICATIONS

A. Hydrogen atom in linearly polarized laser fields

As a demonstration, we consider a hydrogen atom irradiated by a few-cycle linearly polarized infrared laser pulse. The vector potential of the laser field is

$$A = -\frac{A_0}{\omega} \sin^2\left(\frac{\pi t}{t_p}\right) \sin(\omega t)\vec{e}_z, \tag{9}$$

where $t_p = \frac{4\pi}{\omega}$. The laser field is present between $t = 0$ and $t = t_p$, and $\vec{e}_z$ is the unit vector pointing in the polarization direction. The electric field is obtained by $\vec{F} = -\frac{1}{c}\frac{\partial A}{\partial(t)}$.

1. Ring-source semiclassical trajectories

We use the shooting method to obtain semiclassical trajectories for a given final momentum under the constraint of saddle-point conditions given by Eq. (4). Our numerical results show that there are infinitely many semiclassical trajectories deflected by the combined Coulomb potential and laser field into the same final momentum. In Figs. 1(a) and 1(b), we draw some typical trajectories of the electron in coordinate space as well as momentum space, and all of these trajectories reach the same final momenta of $p_{zf} = 0.66$ a.u., $p_{xf} = 0.12$ a.u., and $p_{yf} = 0$ when $t_f \to \infty$. From Figs. 1(c) and 1(d), we see interestingly that the initial momenta of these semiclassical trajectories are distributed in a ring, and the initial coordinates are no longer on the z axis and show a symmetric double-ring structure. After the acceleration of the laser field and the scattering of the nuclear Coulomb potential, these photoelectrons are finally scattered into the same final momentum [see Fig. 1(b)].

Figures 2(a) and 2(b) show the initial transverse momentum $p_{\rho 0}$, position ρ_0, and azimuthal angle ϕ_0 with respect to final transverse momentum p_{xf} for the fixed final momenta $p_{zf} = 0.6$ a.u., $p_{yf} = 0$. When final transverse momenta p_{xf} tend to zero, the initial transverse momentum becomes independent on ϕ_0, and the initial positions ρ_0 tend to zero. This corresponds to a glory rescattering trajectory as shown in Fig. 2(c). For small p_{xf} of 0.03 a.u., in Fig. 2(d), we also draw the joint distribution of the initial positions and initial momenta of photoelectron trajectories, which forms a ring source similar to that of Fig. 1.

Interestingly, with increasing the transverse final momentum more (>0.16 a.u.), our calculations show some classical trajectory forbidden regions denoted by the black areas in Figs. 2(a) and 2(b). For instance, we plot, for the case of $p_{xf} = 0.2$ a.u., the initial transverse momenta of photoelectron trajectories in Fig. 2(e) and the initial positions on the x-y plane Fig. 2(f). In our calculations, we confine our initial positions of tunneling electrons within 16 a.u. distance to the z axis. To apply our UGRT to these situations, we need to make the analytical extension of the solutions to the forbidden regions, as indicated by the dashed lines in Figs. 2(e) and 2(f).

2. Calculations of PMDs

To validate our theory, we also solve the time-dependent Schrödinger equation of a hydrogen atom in an infrared few-cycle linearly polarized laser field with a generalized pseudospectral method [61]. The corresponding Hamiltonian is $H[\vec{r}(t), \vec{p}(t)] = \frac{p^2(t)}{2} + \vec{F}(t)\cdot\vec{r}(t) - \frac{1}{r(t)}$.

In Fig. 3, we compare our theoretical results with the TDSE for varied laser wavelengths. From Figs. 3(a) and 3(b) we can clearly see that the fringes calculated using UGRT are highly consistent with the results of the TDSE. UGRT can precisely predict the positions of interference fringes even for the large scattering angles. In the present numerical simulation, we focus on holographic interference. Therefore, we use a few-cycle laser pulse to reduce intercycle interference. The soft recollision is also prohibited in this case, and the low-energy structure [62] is not apparent. The one-dimensional (1D) slices of PMDs at the fixed final momenta p in Figs. 3(c) and 3(d) show that the results of UGRT can also quantitatively predict the scattering amplitudes. As a comparison, the GRT can only give a good prediction inside the first scattering minimum but fails to predict both fringe positions and scattering amplitudes for the higher-order fringes.

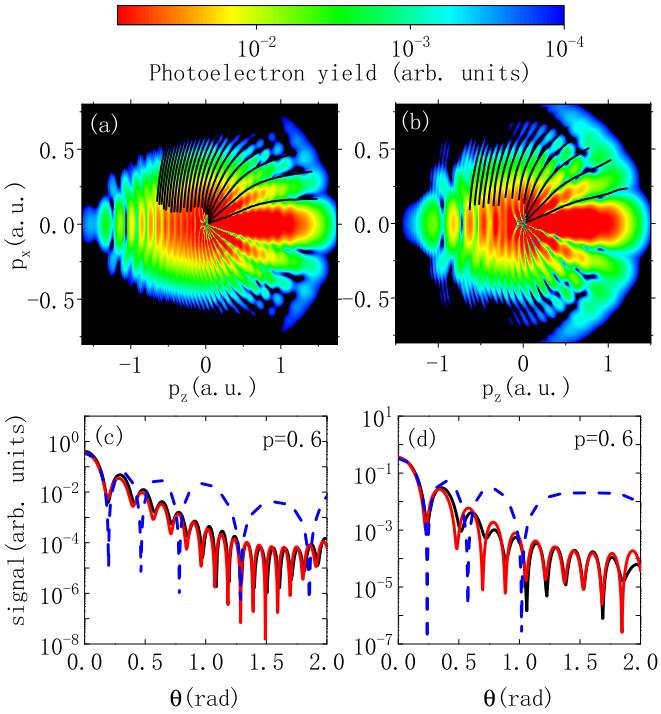

FIG. 3. [(a) and (b)] The PMDs for the hydrogen ionized by laser pulses with 8.7×10^{13} W/cm^2 intensity calculated by TDSE, and the interference fringes predicted by our UGRT (black lines). [(c) and (d)] The momentum distributions corresponding to fixed final momenta $p = 0.6$ a.u. from calculations of TDSE (solid black lines), UGRT (solid red lines), and GRT (dashed blue lines), respectively. The wavelength of laser pulses are [(a) and (c)] $\lambda = 1600$ nm and [(b) and (d)] $\lambda = 1200$ nm . In (c) and (d), scattering angle $\theta = \arctan(\frac{p_{\rho f}}{p_{zf}})$.

For the small scattering angle, the scattering amplitude predicted by the two-trajectory interference models (even with Gouy's phase modification) diverges because the prefactor $\det(\frac{\partial \vec{p}_s}{\partial \vec{p}_f})$ there tends to infinity [39]. In our UGRT and GRT, the presence of the term of the square root of the phase difference in the prefactor [see Eq. (7)] will eliminate this singularity. When the final transverse momentum is large, i.e., for the large scattering angles, the phase differences increase. The Bessel functions then reduce to the simple cosine functions in the asymptotical forms of $J_\alpha(x) \to \sqrt{\frac{2}{\pi x}}\cos(x - \frac{\alpha\pi}{2} - \frac{\pi}{4})$, where α is the order of the Bessel function.

B. Application to experiment of xenon

We now apply our theory to the experiment of xenon [the red lines in Fig. 4(a) and black squares in Fig. 4(b)]. The

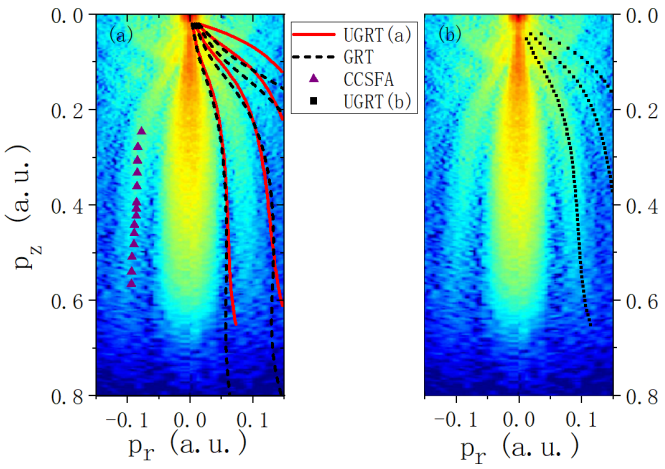

FIG. 4. Experimental holographic pattern and positions of the dark fringes calculated by UGRT [red lines in (a)], GRT (dashed black lines), and CCSFA (purple triangles). Positions of the bright fringes calculated by UGRT [black squares in (b)]. The experimental data are extracted from Ref. [8], where the metastable ($6s$) Xe atoms with ionization potential of 0.14 a.u. are ionized with linearly polarized mid-infrared laser pulses with duration of 5 to 20 cycles. The laser parameters are $\lambda = 7\ \mu$m and $I = 7.1 \times 10^{11}$ W/cm^2.

experiments of metastable ($6s$) Xe atoms in this figure are using mid-IR laser pulses with the wavelength of 7000 nm [8]. We calculated cases with pulse duration varied from 5 to 20 cycles. No significant changes of fringe spacing are observed when the pulse duration is varied. In Fig. 4 we show the theoretical results of a five-cycle laser pulse. The positions of bright and dark fringes predicted by our theory are in good agreement with the experimental results. As a comparison, we also plot the results predicted by other theories such as GRT (black dash) and CCSFA (purple solid triangles). According to CCSFA, the coherent summation of the two paths leads to cos ΔS-type oscillations in holography patterns. However, infinitely many semiclassical paths can approach the same final momentum, and the quantum interference of these trajectories will dominate the holographic fringe structure. Our UGRT takes into account the contributions of these infinitely many trajectories by properly dealing with the integration over the azimuthal angle using uniform approximation. We can see that CCSFA even fails to predict the position of the first dark fringe, while GRT and UGRT are in perfect agreement with the experiment in this region. However, the discrepancy between the GRT and UGRT becomes more apparent for the third- or higher-order fringes. We hope that these theoretical predictions can be calibrated in the future by SFPH experiments with higher resolution.

IV. CONCLUSIONS

We investigate the PMDs of the ionized atoms irradiated by a linearly polarized strong laser field and provide a semiclassical trajectory perspective of glory rescattering in SFPH. We calculate the scattering amplitudes in the cylindrical coordinate representation and finally derive a uniform formulation in the Bessel functions for the SFPH patterns. Our results are also in good agreement with solutions of the TDSE calculations and can give explanations for recent photoelectron holography experiments of Xe atoms. Compared with existing theories (see Table II), our UGRT provides a distinct ring-source infinite-trajectory interference description for photoelectron holograph patterns analogous to ring-source diffraction in optics. Our results of uniform approximation can also be applied to molecule and nondipole situations. Our further calculations show that the theory can be generalized to initial states other than s states; related works are ongoing. Our work therefore has important implications in both theoretical aspects and the practical applications of SFPH.

ACKNOWLEDGMENTS

This work is supported by the National Natural Science Foundation of China (Grants No. 11775030 and No. 11974057) and NSAF (Grant No. U1930403).

APPENDIX A: UNIFORM APPROXIMATION

From Eq. (5) we can see that the phase $\mathcal{A}_s$ is the implicit function of the azimuthal angle ϕ. To treat this scattering amplitude integration, we closely follow Berry's spirit of uniform approximation [43,44] with renormalizing the angular variable. Let us introduce a new angular variable φ, which satisfies $\phi = 0 \leftrightarrow \varphi = 0$, $\phi = \pi \leftrightarrow \varphi = \pi$, and $\mathcal{A}_s(\phi) = \bar{\mathcal{A}}_s(\varphi) \equiv \mathcal{A}_0 + \mathcal{A}_1 \cos(\varphi)$, where $\mathcal{A}_0 = (\mathcal{A}_s(\phi = 0) + \mathcal{A}_s(\phi = \pi))/2$ corresponds to the sum of the phases of the $\phi = 0$ and $\phi = \pi$ semiclassical photoelectron trajectories, and $\mathcal{A}_1 = (\mathcal{A}_s(\phi = 0) - \mathcal{A}_s(\phi = \pi))/2$ corresponds to the phase difference between the $\phi = 0$ and $\phi = \pi$ trajectories. Further, we can get

$$\frac{d\phi}{d\varphi} = \frac{d\bar{\mathcal{A}}_s}{d\varphi} \Big/ \frac{d\mathcal{A}_s}{d\phi} = \frac{\mathcal{A}_1 \sin\varphi}{L_\phi}, \tag{A1}$$

where $L_\phi = -\frac{d\mathcal{A}}{d\phi}$ is the photoelectron angular momentum along the polarization direction. For a linearly polarized laser field, the mirror symmetry will lead to $\frac{d\mathcal{A}_s}{d\phi} = 0$ at $\phi = 0$ and

TABLE II. Optical analogs of SFPH theories (ΔS denotes the phase difference of semiclassical trajectories).

Theory	Interference picture	Interference formula	Optical analogs
Conventional models	Two-trajectory interference	$\cos(\Delta S)$	Double slit interference
UGRT	Ring-source infinitely many trajectories	$C_0 J_0(\Delta S) + C_1 J_1(\Delta S)$	Ring-source diffraction
GRT	Point-source infinitely many trajectories	$J_0(\Delta S)$	Point-source diffraction

π. Both the denominator and numerator in Eq. (A1) become zeros when $\phi = 0$ and π. Using L'Hospital's rule, we have

$$\frac{d\phi}{d\varphi} = \frac{d(\mathcal{A}_1 \sin\varphi)/d\phi}{dL_\phi/d\phi} = \frac{d(\mathcal{A}_1 \sin\varphi)/d\varphi}{dL_\phi/d\phi} \Big/ \left(\frac{d\phi}{d\varphi}\right), \tag{A2}$$

$$\frac{d\phi}{d\varphi} = \left(\mathcal{A}_1 \cos\varphi \Big/ \frac{dL_\phi}{d\phi}\right)^{\frac{1}{2}}. \tag{A3}$$

With the variable transformation, the scattering amplitude of Eq. (5) turns out to be

$$M_{\vec{p}_f} \approx \int_0^{2\pi} d\varphi C(\varphi) e^{i(\mathcal{A}_0 + \mathcal{A}_1 \cos\varphi)}, \tag{A4}$$

where $C(\varphi)$ is the prefactor in the scattering amplitude integral which takes the following form:

$$C(\varphi) = e^{i\mathcal{A}_0} \mathcal{F}_s \mathcal{D}_s p_{\rho_s} \left(\frac{\partial^2 \mathcal{A}_s}{\partial t_s^2}\right)^{-\frac{1}{2}} \left(\frac{(2\pi i)^3 \mathcal{A}_1 \cos\varphi}{\frac{dL_\phi}{d\phi} \det\left(\frac{\partial^2 \mathcal{A}_s}{\partial(p_{zs}, p_{\rho s})}\right)}\right)^{\frac{1}{2}}, \tag{A5}$$

where $\frac{dL_\phi}{d\phi} = -\frac{d^2\mathcal{A}_s}{d\phi_0^2}$. When $\varphi = 0$ and $\varphi = \pi$, we can prove the property that (proved in Appendix B)

$$\frac{d^2\mathcal{A}_s}{d\phi_0^2} \det \frac{\partial^2 \mathcal{A}_s}{\partial(p_{\rho s}, p_{zs})} = \det\left(\frac{\partial^2 \mathcal{A}_s}{\partial(p_{zs}, p_{\rho s}, \phi_0)}\right). \tag{A6}$$

Furthermore,

$$p_{\rho s}^2 / \det\left(\frac{\partial^2 \mathcal{A}_s}{\partial(p_{zs}, p_{\rho s}, \phi_0)}\right) = \left(\det\left(\frac{\partial^2 \mathcal{A}_s}{\partial \vec{p}_s^{\,2}}\right)\right)^{-1}. \tag{A7}$$

In the semiclassical model, the prefactor $\mathcal{F}_s \propto (\det(\frac{\partial^2 \mathcal{A}_s}{\partial \vec{p}_s \partial \vec{p}_f}))^{\frac{1}{2}}$. We can combine the two determinants in Eq. (A5), $\det(\frac{\partial^2 \mathcal{A}_s}{\partial \vec{p}_s \partial \vec{p}_f}))^{\frac{1}{2}} (\det(\frac{\partial^2 \mathcal{A}_s}{\partial \vec{p}_s^{\,2}}))^{-1} = \det(\frac{\partial \vec{p}_s}{\partial \vec{p}_f})$.

Under the cylindrical symmetry of linearly polarized fields, we have

$$\det\left(\frac{\partial \vec{p}_s}{\partial \vec{p}_f}\right) = \frac{p_{\rho s}}{p_{\rho f}} \det\left(\frac{\partial(p_{zs}, p_{\rho s})}{\partial(p_{zf}, p_{\rho f})}\right). \tag{A8}$$

Substituting Eq. (A8) into Eq. (A5), we get the prefactor of the following form:

$$C(\varphi) \propto \frac{\mathcal{D}_s}{\sqrt{\frac{d^2\mathcal{A}_s}{dt_s^2}}} (\mathcal{A}_1 \cos\varphi)^{\frac{1}{2}} \frac{p_{\rho s}}{p_{\rho f}} \det\left(\frac{\partial(p_{zs}, p_{\rho s})}{\partial(p_{zf}, p_{\rho f})}\right). \tag{A9}$$

Based on the above derivation, we can approximate the scattering amplitude integral in cylindrical coordinates to the form expressed by Bessel functions, and finally get Eq. (8).

APPENDIX B: DERIVATION OF EQ. (A6)

Under the saddle-point condition of our derivation,

$$\frac{\partial \mathcal{A}_s}{\partial p_{z0}} = 0, \quad \frac{\partial \mathcal{A}_s}{\partial p_{\rho 0}} = 0. \tag{B1}$$

Differentiating the above equations, we get

$$\begin{aligned} d\left(\frac{\partial \mathcal{A}_s}{\partial p_{z0}}\right) &= \frac{\partial^2 \mathcal{A}_s}{\partial p_{z0}^2} dp_{z0} + \frac{\partial^2 \mathcal{A}_s}{\partial p_{z0} \partial p_{\rho 0}} dp_{\rho 0} + \frac{\partial^2 \mathcal{A}_s}{\partial p_{z0} \partial \phi_0} d\phi_0 \\ &= 0, \\ d\left(\frac{\partial \mathcal{A}_s}{\partial p_{\rho 0}}\right) &= \frac{\partial^2 \mathcal{A}_s}{\partial p_{\rho 0}^2} dp_{\rho 0} + \frac{\partial^2 \mathcal{A}_s}{\partial p_{z0} \partial p_{\rho 0}} dp_{z0} + \frac{\partial^2 \mathcal{A}_s}{\partial p_{\rho 0} \partial \phi_0} d\phi_0 \\ &= 0. \end{aligned} \tag{B2}$$

According to the total differential formula, we have the following properties:

$$\begin{aligned} d^2\mathcal{A}_s = &\frac{\partial^2 \mathcal{A}_s}{\partial p_{z0}^2} dp_{z0}^2 + \frac{\partial^2 \mathcal{A}_s}{\partial p_{\rho 0}^2} dp_{\rho 0}^2 + \frac{\partial^2 \mathcal{A}_s}{\partial \phi_0^2} d\phi_0^2 \\ &+ 2\frac{\partial^2 \mathcal{A}_s}{\partial p_{z0} \partial p_{\rho 0}} dp_{z0} dp_{\rho 0} + 2\frac{\partial^2 \mathcal{A}_s}{\partial p_{\rho 0} \partial \phi_0} dp_{\rho 0} d\phi_0 \\ &+ 2\frac{\partial^2 \mathcal{A}_s}{\partial \phi_0 \partial p_{z0}} d\phi_0 dp_{z0}. \end{aligned} \tag{B3}$$

Using the above properties we can get the property of Eq. (A6) we need in Appendix A,

$$\begin{aligned} \det\left(\frac{\partial^2 \mathcal{A}_s}{\partial(p_{z0}, p_{\rho 0})}\right) \frac{d^2\mathcal{A}_s}{d\phi_0^2} &= \left(\frac{\partial^2 \mathcal{A}_s}{\partial p_{z0}^2} \frac{\partial^2 \mathcal{A}_s}{\partial p_{\rho 0}^2} - \left(\frac{\partial^2 \mathcal{A}_s}{\partial p_{z0} \partial p_{\rho 0}}\right)^2\right) \\ &\times \left(\frac{\partial^2 \mathcal{A}_s}{\partial \phi_0^2} + \frac{\partial^2 \mathcal{A}_s}{\partial p_{\rho 0} \partial \phi_0} \frac{dp_{\rho 0}}{d\phi_0} + \frac{\partial^2 \mathcal{A}_s}{\partial \phi_0 \partial p_{z0}} \frac{dp_{z0}}{d\phi_0}\right) \\ &= \frac{\partial^2 \mathcal{A}_s}{\partial p_{z0}^2} \frac{\partial^2 \mathcal{A}_s}{\partial p_{\rho 0}^2} \frac{\partial^2 \mathcal{A}_s}{\partial \phi_0^2} - \left(\frac{\partial^2 \mathcal{A}_s}{\partial p_{z0} \partial p_{\rho 0}}\right)^2 \frac{\partial^2 \mathcal{A}_s}{\partial \phi_0^2} \\ &- \left(\frac{\partial^2 \mathcal{A}_s}{\partial p_{z0} \partial \phi_0}\right)^2 \frac{\partial^2 \mathcal{A}_s}{\partial p_{\rho 0}^2} - \left(\frac{\partial^2 \mathcal{A}_s}{\partial p_{\rho 0} \partial \phi_0}\right)^2 \frac{\partial^2 \mathcal{A}_s}{\partial p_{z0}^2} \\ &+ 2\frac{\partial^2 \mathcal{A}_s}{\partial p_{\rho 0} \partial \phi_0} \frac{\partial^2 \mathcal{A}_s}{\partial p_{z0} \partial p_{\rho 0}} \frac{\partial^2 \mathcal{A}_s}{\partial p_{z0} \partial \phi_0} \\ &= \det\left(\frac{\partial^2 \mathcal{A}_s}{\partial(p_{z0}, p_{\rho 0}, \phi_0)}\right). \end{aligned} \tag{B4}$$

[1] F. Lindner, M. G. Schätzel, H. Walther, A. Baltuška, E. Goulielmakis, F. Krausz, D. B. Milošević, D. Bauer, W. Becker, and G. G. Paulus, Attosecond Double-Slit Experiment, Phys. Rev. Lett. **95**, 040401 (2005).

[2] R. Gopal, K. Simeonidis, R. Moshammer, T. Ergler, M. Dürr, M. Kurka, K. U. Kühnel, S. Tschuch, C. D. Schröter, D. Bauer, J. Ullrich, A. Rudenko, O. Herrwerth, T. Uphues, M. Schultze, E. Goulielmakis, M. Uiberacker, M. Lezius, and M. F. Kling, Three-Dimensional Momentum Imaging of Electron Wave Packet Interference in Few-Cycle Laser Pulses, Phys. Rev. Lett. **103**, 053001 (2009).

[3] Y. Huismans, A. Rouzée, A. Gijsbertsen, J. Jungmann, A. Smolkowska, P. Logman, F. Lepine, C. Cauchy, S. Zamith, T. Marchenko *et al.*, Time-resolved holography with photoelectrons, Science **331**, 61 (2011).

[4] X. B. Bian, Y. Huismans, O. Smirnova, K. J. Yuan, M. Vrakking, and A. D. Bandrauk, Subcycle interference dynamics of time-resolved photoelectron holography with midinfrared laser pulses, Phys. Rev. A **84**, 043420 (2011).

[5] P. A. Korneev, S. V. Popruzhenko, S. P. Goreslavski, T. M. Yan, D. Bauer, W. Becker, M. Kübel, M. F. Kling, C. Rödel, M. Wünsche, and G. G. Paulus, Interference Carpets in Above-Threshold Ionization: From the Coulomb-Free to the Coulomb-Dominated Regime, Phys. Rev. Lett. **108**, 223601 (2012).

[6] X. Xie, S. Roither, D. Kartashov, E. Persson, D. G. Arbó, L. Zhang, S. Gräfe, M. S. Schöffler, J. Burgdörfer, A. Baltuška, and M. Kitzler, Attosecond Probe of Valence-Electron Wave Packets by Subcycle Sculpted Laser Fields, Phys. Rev. Lett. **108**, 193004 (2012).

[7] X. B. Bian and A. D. Bandrauk, Attosecond Time-Resolved Imaging of Molecular Structure by Photoelectron Holography, Phys. Rev. Lett. **108**, 263003 (2012).

[8] Y. Huismans, A. Gijsbertsen, A. S. Smolkowska, J. H. Jungmann, A. Rouzée, P. S. W. M. Logman, F. Lépine, C. Cauchy, S. Zamith, T. Marchenko, J. M. Bakker, G. Berden, B. Redlich, A. F. G. van der Meer, M. Y. Ivanov, T. M. Yan, D. Bauer, O. Smirnova, and M. J. J. Vrakking, Scaling Laws for Photoelectron Holography in the Midinfrared Wavelength Regime, Phys. Rev. Lett. **109**, 013002 (2012).

[9] D. D. Hickstein, P. Ranitovic, S. Witte, X. M. Tong, Y. Huismans, P. Arpin, X. Zhou, K. E. Keister, C. W. Hogle, B. Zhang, C. Ding, P. Johnsson, N. Toshima, M. J. J. Vrakking, M. M. Murnane, and H. C. Kapteyn, Direct Visualization of Laser-Driven Electron Multiple Scattering and Tunneling Distance in Strong-Field Ionization, Phys. Rev. Lett. **109**, 073004 (2012).

[10] M. Meckel, A. Staudte, S. Patchkovskii, D. Villeneuve, P. Corkum, R. Dörner, and M. Spanner, Signatures of the continuum electron phase in molecular strong-field photoelectron holography, Nat. Phys. **10**, 594 (2014).

[11] M. Haertelt, X. B. Bian, M. Spanner, A. Staudte, and P. B. Corkum, Probing Molecular Dynamics by Laser-Induced Backscattering Holography, Phys. Rev. Lett. **116**, 133001 (2016).

[12] S. G. Walt, N. B. Ram, M. Atala, N. I. Shvetsov-Shilovski, A. Von Conta, D. Baykusheva, M. Lein, and H. J. Wörner, Dynamics of valence-shell electrons and nuclei probed by strong-field holography and rescattering, Nat. Commun. **8**, 15651 (2017).

[13] C. F. D. M. Faria and A. S. Maxwell, It is all about phases: Ultrafast holographic photoelectron imaging, Rep. Prog. Phys. **83**, 034401 (2020).

[14] N. Werby, A. S. Maxwell, R. Forbes, P. H. Bucksbaum, and C. F. D. M. Faria, Dissecting subcycle interference in photoelectron holography, Phys. Rev. A **104**, 013109 (2021).

[15] P. B. Corkum and F. Krausz, Attosecond science, Nat. Phys. **3**, 381 (2007).

[16] P. B. Corkum, Recollision physics, Phys. Today **64**(3), 36 (2011).

[17] H. Kang, A. S. Maxwell, D. Trabert, X. Lai, S. Eckart, M. Kunitski, M. Schöffler, T. Jahnke, X. Bian, R. Dörner, and C. F. D. M. Faria, Holographic detection of parity in atomic and molecular orbitals, Phys. Rev. A **102**, 013109 (2020).

[18] P. B. Corkum, N. H. Burnett, and F. Brunel, Above-Threshold Ionization in the Long-Wavelength Limit, Phys. Rev. Lett. **62**, 1259 (1989).

[19] P. B. Corkum, Plasma Perspective on Strong Field Multiphoton Ionization, Phys. Rev. Lett. **71**, 1994 (1993).

[20] J. M. Rost, Semiclassical S-matrix theory for atomic fragmentation, Phys. Rep. **297**, 271 (1998).

[21] G. van de Sand and J. M. Rost, Semiclassical description of multiphoton processes, Phys. Rev. A **62**, 053403 (2000).

[22] J. Liu, *Classical Trajectory Perspective of Atomic Ionization in Strong Laser Fields: Semiclassical Modeling* (Springer, Berlin, 2013).

[23] M. Lewenstein, K. C. Kulander, K. J. Schafer, and P. H. Bucksbaum, Rings in above-threshold ionization: A quasiclassical analysis, Phys. Rev. A **51**, 1495 (1995).

[24] T. M. Yan and D. Bauer, Sub-barrier Coulomb effects on the interference pattern in tunneling-ionization photoelectron spectra, Phys. Rev. A **86**, 053403 (2012).

[25] M. Li, X. Sun, X. Xie, Y. Shao, Y. Deng, C. Wu, Q. Gong, and Y. Liu, Revealing backward rescattering photoelectron interference of molecules in strong infrared laser fields, Sci. Rep. **5**, 8519 (2015).

[26] S. Brennecke and M. Lein, Strong-field photoelectron holography beyond the electric dipole approximation: A semiclassical analysis, Phys. Rev. A **100**, 023413 (2019).

[27] S. D. López and D. G. Arbó, Holographic interference in atomic photoionization from a semiclassical standpoint, Phys. Rev. A **100**, 023419 (2019).

[28] D. Bauer and P. Koval, Qprop: A Schrödinger-solver for intense laser-atom interaction, Comput. Phys. Commun. **174**, 396 (2006).

[29] Q. Li, X. M. Tong, T. Morishita, H. Wei, and C. D. Lin, Fine structures in the intensity dependence of excitation and ionization probabilities of hydrogen atoms in intense 800-nm laser pulses, Phys. Rev. A **89**, 023421 (2014).

[30] L. V. Keldysh, Ionization in the field of a strong electromagnetic wave, Sov. Phys. JETP **20**, 1307 (1965).

[31] F. H. M. Faisal, Multiple absorption of laser photons by atoms, J. Phys. B: At. Mol. Phys. **6**, L89 (1973).

[32] H. R. Reiss, Effect of an intense electromagnetic field on a weakly bound system, Phys. Rev. A **22**, 1786 (1980).

[33] S. Popruzhenko and D. Bauer, Strong field approximation for systems with Coulomb interaction, J. Mod. Opt. **55**, 2573 (2008).

[34] S. V. Popruzhenko, G. G. Paulus, and D. Bauer, Coulomb-corrected quantum trajectories in strong-field ionization, Phys. Rev. A **77**, 053409 (2008).

[35] T. M. Yan, S. V. Popruzhenko, M. J. J. Vrakking, and D. Bauer, Low-Energy Structures in Strong Field Ionization Revealed by Quantum Orbits, Phys. Rev. Lett. **105**, 253002 (2010).

[36] S. V. Popruzhenko, Keldysh theory of strong field ionization: History, applications, difficulties and perspectives, J. Phys. B: At. Mol. Opt. Phys. **47**, 204001 (2014).

[37] L. G. Gouy, Sur une propriété nouvelle des ondes lumineuses, C. R. Acad. Sci. Paris **110**, 1251 (1890).

[38] M. C. Gutzwiller, *Chaos in Classical and Quantum Mechanics* (Springer, Berlin, 2013), Vol. 1.

[39] S. Brennecke, N. Eicke, and M. Lein, Gouy's Phase Anomaly in Electron Waves Produced by Strong-Field Ionization, Phys. Rev. Lett. **124**, 153202 (2020).

[40] P. Sikivie, Caustic ring singularity, Phys. Rev. D **60**, 063501 (1999).

[41] H. M. Nussenzveig, *Diffraction Effects in Semiclassical Scattering* (Cambridge University Press, Cambridge, U.K., 2006), Vol. 1.

[42] Q. Z. Xia, J. F. Tao, J. Cai, L. B. Fu, and J. Liu, Quantum Interference of Glory Rescattering in Strong-Field Atomic Ionization, Phys. Rev. Lett. **121**, 143201 (2018).
[43] M. V. Berry, Uniform approximation: A new concept in wave theory, Sci. Prog. (1933-) **57**, 43 (1969).
[44] M. V. Berry, Uniform approximations for glory scattering and diffraction peaks, J. Phys. B: At. Mol. Phys. **2**, 381 (1969).
[45] F. J. Dyson, The *S* matrix in quantum electrodynamics, Phys. Rev. **75**, 1736 (1949).
[46] M. C. Gutzwiller, Phase-integral approximation in momentum space and the bound states of an atom, J. Math. Phys. **8**, 1979 (1967).
[47] D. B. Milošević, Semiclassical approximation for strong-laser-field processes, Phys. Rev. A **96**, 023413 (2017).
[48] M. V. Berry, Nature's optics and our understanding of light, Contemp. Phys. **56**, 2 (2015).
[49] K. W. Ford and J. A. Wheeler, Semiclassical description of scattering, Ann. Phys. **7**, 259 (1959).
[50] J. A. Adam, The mathematical physics of rainbows and glories, Phys. Rep. **356**, 229 (2002).
[51] L. Torlina and O. Smirnova, Time-dependent analytical *R*-matrix approach for strong-field dynamics. I. One-electron systems, Phys. Rev. A **86**, 043408 (2012).
[52] J. Kaushal and O. Smirnova, Nonadiabatic Coulomb effects in strong-field ionization in circularly polarized laser fields, Phys. Rev. A **88**, 013421 (2013).
[53] D. B. Milošević, G. G. Paulus, D. Bauer, and W. Becker, Above-threshold ionization by few-cycle pulses, J. Phys. B: At. Mol. Opt. Phys. **39**, R203 (2006).
[54] M. Li, J. W. Geng, M. Han, M. M. Liu, L. Y. Peng, Q. Gong, and Y. Liu, Subcycle nonadiabatic strong-field tunneling ionization, Phys. Rev. A **93**, 013402 (2016).
[55] D. D. Morrison, J. D. Riley, and J. F. Zancanaro, Multiple shooting method for two-point boundary value problems, Commun. ACM **5**, 613 (1962).
[56] N. I. Shvetsov-Shilovski, M. Lein, L. B. Madsen, E. Räsänen, C. Lemell, J. Burgdörfer, D. G. Arbó, and K. Tőkési, Semiclassical two-step model for strong-field ionization, Phys. Rev. A **94**, 013415 (2016).
[57] K. Möhring, S. Levit, and U. Smilansky, On the semiclassical Green's function in the energy-representation, Ann. Phys. **127**, 198 (1980).
[58] M. L. Du and J. Delos, Effect of Closed Classical Orbits on Quantum Spectra: Ionization of Atoms in a Magnetic Field, Phys. Rev. Lett. **58**, 1731 (1987).
[59] V. P. Maslov and M. V. Fedoriuk, *Semi-classical Approximation in Quantum Mechanics* (Springer, Berlin, 2001), Vol. 7.
[60] J. B. Delos, Semiclassical calculation of quantum mechanical wave functions, Adv. Chem. Phys. **65**, 161 (1986).
[61] X. M. Tong and S. I. Chu, Theoretical study of multiple high-order harmonic generation by intense ultrashort pulsed laser fields: A new generalized pseudospectral time-dependent method, Chem. Phys. **217**, 119 (1997).
[62] C. I. Blaga, F. Catoire, P. Colosimo, G. G. Paulus, H. G. Muller, P. Agostini, and L. F. DiMauro, Strong-field photoionization revisited, Nat. Phys. **5**, 335 (2009).